

Non-Markovian enhanced temperature sensing in a dipolar Bose-Einstein condensateLan Xu ¹, Ji-Bing Yuan,² Shi-Qing Tang,² Wei Wu,³ Qing-Shou Tan ^{4,*} and Le-Man Kuang^{5,6}¹*School of Physics and Chemistry, Hunan First Normal University, Changsha 410205, China*²*Department of Physics and Electronic Information Science, Hengyang Normal University, Hengyang 421002, China*³*Key Laboratory of Theoretical Physics of Gansu Province, and Lanzhou Center for Theoretical Physics, Lanzhou University, Lanzhou 730000, China*⁴*Key Laboratory of Hunan Province on Information Photonics and Freespace Optical Communication, College of Physics and Electronics, Hunan Institute of Science and Technology, Yueyang 414000, China*⁵*Key Laboratory of Low-Dimensional Quantum Structures and Quantum Control of Ministry of Education, Department of Physics and Synergetic Innovation Center for Quantum Effects and Applications, Hunan Normal University, Changsha 410081, China*⁶*Synergetic Innovation Academy for Quantum Science and Technology, Zhengzhou University of Light Industry, Zhengzhou 450002, China*

(Received 30 April 2023; revised 13 July 2023; accepted 28 July 2023; published 10 August 2023)

We present a method for implementing quantum temperature sensing for extremely low temperatures in a quasi-1D dipolar Bose-Einstein condensate reservoir with a magnetic field-driven impurity atom acting as a quantum sensor. By analyzing the quantum signal-to-noise ratio (QSNR) as a metric for temperature sensing performance, we demonstrate that the presence of an attractive dipolar interaction in the reservoir, which includes the effects of non-Markovian dynamics on the sensor, significantly enhances estimation efficiency. We also investigate the steady-state estimation efficiency for long-encoding times through an analytical expression, which shows that the optimal QSNR depends on the driving magnetic field of the impurity atom. Our method can achieve high-efficiency temperature sensing for any low temperature by tuning the magnetic field. These findings suggest that our approach has potential applications in high-resolution quantum thermometry.

DOI: [10.1103/PhysRevA.108.022608](https://doi.org/10.1103/PhysRevA.108.022608)**I. INTRODUCTION**

Temperature is a fundamental concept in both classical and quantum thermodynamics. In particular, achieving an ultralow temperature is crucial for quantum simulation and computation [1]. Although cold atomic gases have been cooled to the sub-nK regime, accurately measuring such low temperatures in a nondestructive manner remains a challenging task [2–5]. This is due to both the complexity of the required experimental setup and fundamental limitations in precision. To overcome these challenges, a good thermometer should be so small that it does not significantly disturb the temperature of the bath during the measurement process. One approach is to use a quantum sensor such as a two-level system [6–11] or harmonic oscillator [12–14] that is coupled to the quantum reservoir to encode the temperature information. By measuring the sensor's observables, we can obtain knowledge of the temperature without disturbing the bath. Moreover, quantum temperature sensors can potentially revolutionize temperature measurement by utilizing coherence, quantum squeezing, entanglement, or other quantum resources to achieve a level of precision that surpasses the standard bound set by classical statistics [15,16]. With their high precision and sensitivity, these sensors have the potential to improve temperature measurement.

Research on quantum thermometers can generally be classified into two main types: fully thermalized thermometers

[17–19] and partly thermalized thermometers [20,21]. In the case of thermal equilibrium probes, where the probes are in thermal equilibrium with the sample and temperature sensing accuracy is determined by the heat capacity, it has been demonstrated that the sensing error will exponentially increase as the temperature approaches zero [22,23]. However, for nonthermal equilibrium probes, where the quantum probes do not equilibrate with the sample but in a nonthermal steady state, the sensing error will still increase, but the divergence will be polynomial rather than exponential [24,25]. Currently, numerous attempts are made to tackle the issue of error divergence in quantum temperature sensing, such as the utilization of harmonic oscillator probes. Reference [12] reported that by employing a Brownian particle as a temperature sensor for a Bose-Einstein condensate (BEC) reservoir, the relative error for temperatures as low as 200 pK can be kept below 14% for as few as 100 measurements. Nonetheless, research of high-sensitivity temperature sensing utilizing a qubit probe in the BEC system is still ongoing.

Recently, studies have shown that non-Markovian effects can significantly impact the effectiveness of quantum sensing [26–29]. In particular, in a dipolar BEC system, non-Markovian effects can be regulated due to the tunable magnetic dipole-dipole interaction (MDDI) [30–35], allowing for the study of non-Markovian dynamics in a controlled manner [36–38]. Additionally, impurities in the system can lead to interesting effects on the dynamics. Understanding their impact is essential for developing high-precision quantum temperature sensing.

*qstan@hnist.edu.cn

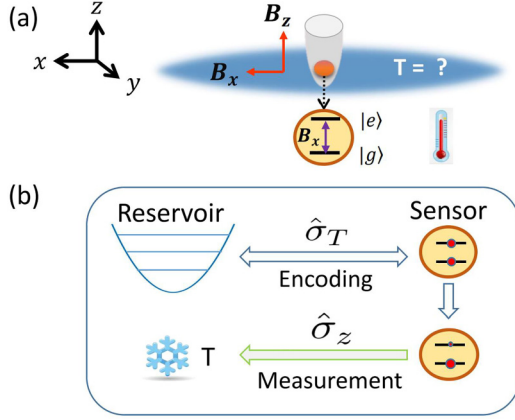


FIG. 1. (a) The physical system of the quantum temperature sensing under consideration. An atomic qubit is immersed in a thermally equilibrated quasi-1D dipolar BEC, which acts as a quantum sensor to estimate the temperature of the BEC reservoir. (b) Scheme of our proposed thermometry protocol, which involves an encoding process and a measurement process.

In this work, we investigate the non-Markovian effects of dipolar BECs on the dynamics of an impurity atom and demonstrate how these effects can enhance the sensitivity of quantum temperature sensors. We use the quantum signal-to-noise ratio (QSNR) as a metric for the performance of temperature sensing and show that the incorporation of attractive dipolar interactions in the reservoir improves the estimation efficiency for partly thermalized thermometers. We also analyze the fully thermalized (steady-state) estimation efficiency using an analytical expression and discover that the optimal QSNR depends on the driving magnetic field of the impurity atom. Our approach takes advantage of the adjustable magnetic field to precisely control the efficiency of estimation at low temperatures.

The paper is structured as follows: In Sec. II, we present the model of atoms immersed in a thermally equilibrated quasi-1D dipolar BEC reservoir and give the dynamics of the atoms under the influence of dissipative noise. In Sec. III, we demonstrate the positive effects of the dipolar interaction in the reservoir as well as the driving magnetic field on the sensitivity of a single-qubit quantum thermometry. Finally, we conclude in Sec. IV.

II. THE MODEL AND DYNAMICS

A. Physical model

We consider a single impurity-atomic qubit that acts as the sensor, immersed in a thermally equilibrated quasi-1D dipolar BEC reservoir at temperature T (shown in Fig. 1). The sensor is confined in a spin-independent, three-dimensional, symmetric harmonic trap $V_a(\mathbf{r}) = m_a \omega_a^2 \mathbf{r}^2 / 2$, with spatial orbital $\Phi_a = (\pi \ell_a^2)^{-3/4} e^{-(x^2+y^2+z^2)/(2\ell_a^2)}$, where $\ell_a = \sqrt{\hbar / (m_a \omega_a)}$, ω_a is the trap frequency, and m_a is the mass. The Hamiltonian of the sensor is then given by

$$H_a = \frac{\hbar \Omega_a}{2} \sigma_z, \quad (1)$$

where $\sigma_z = |e\rangle\langle e| - |g\rangle\langle g|$ and Ω_a is the level splitting between the excited ($|e\rangle$) and ground ($|g\rangle$) states.

For the reservoir atoms, we assume that the dipolar BEC is confined in a cylindrically symmetric trap with a transverse trapping frequency ω_\perp and a negligible longitudinal confinement along the x direction. In three dimensions, the two-body interaction is given by

$$V^{3D}(\mathbf{r}) = g_b \delta(\mathbf{r}) + \frac{3c_d}{4\pi} \frac{1 - 3(\hat{\mu}_m \cdot \hat{\mathbf{r}})^2}{r^3}, \quad (2)$$

where the contact interaction strength is $g_b = 4\pi \hbar^2 a_b / m_b$, with a_b the s -wave scattering length and the dipolar interaction strength is $c_d = 4\pi \hbar^2 a_{dd} / m_b$, where $a_{dd} = \mu_0 \mu_m^2 m_b / (12\pi \hbar^2)$ is a length scale characterizing the dipole-dipole interaction with μ_0 the vacuum permeability, μ_m the magnetic dipole moment, and m_b the mass of the reservoir atom. For sufficiently large ω_\perp , the motion of the atoms along the y - z axis is frozen to the ground state of the oscillator, which is given by $\Psi_\perp(y, z) = (\pi \ell_b^2)^{-1/2} e^{-(y^2+z^2)/(2\ell_b^2)}$, where $\ell_b \equiv \sqrt{\hbar / (m_b \omega_\perp)}$ is the width of the Gaussian function.

Using the Bogoliubov method, the Hamiltonian of the reservoir takes the form [36]

$$H_b = \sum_{k \neq 0} \hbar \omega_k b_k^\dagger b_k, \quad (3)$$

where b_k (b_k^\dagger) is the annihilation (creation) operator of the Bogoliubov modes with momentum k , and the corresponding excitation energy is [38]

$$\omega_k = \frac{1}{2} \omega_\perp \sqrt{(k\ell_b)^4 + \eta(k\ell_b)^2 [1 - \chi \tilde{v}_{1D}(k)]}, \quad (4)$$

where $\eta = 8n_0 a_b$ is a dimensionless parameter depending on the condensate linear density n_0 and the s -wave scattering length a_b . The relative MDDI strength is defined as $\chi \equiv a_{dd} / a_b$, and

$$\tilde{v}_{1D}(k) = 1 - \frac{3}{2} k^2 \ell_b^2 \exp[(k\ell_b)^2 / 2] \Gamma[0, (k\ell_b)^2 / 2] \quad (5)$$

is the Fourier transform of the effective 1D MDDI with $\Gamma(0, x)$ the incomplete Gamma function.

Assuming that the atoms in the reservoir are coupled to the excited state $|e\rangle$ of the sensor (the impurity atom) through a Raman transition, the strength of the coupling depends on the s -wave scattering length a_{ab} , and the interaction Hamiltonian takes the form [36–38]

$$H_{ab} = \hbar \Delta_e \sigma_z + \sigma_z \sum_k \hbar g_k (b_k + b_k^\dagger). \quad (6)$$

Here, $\Delta_e = \hbar a_{ab} n_0 (m_a + m_b) / [m_a m_b (\ell_a^2 + \ell_b^2)]$ and $g_k = \Delta_e \sqrt{\frac{E_k}{n_0 L \hbar \omega_k}} e^{-(k\ell_a)^2 / 4}$, where L is the length of the BEC reservoir. The total interaction between the sensor and the reservoir is described by the Hamiltonian

$$H = \frac{\hbar \delta_a}{2} \sigma_z + \sum_{k \neq 0} \hbar \omega_k b_k^\dagger b_k + \sigma_z \sum_k \hbar g_k (b_k + b_k^\dagger), \quad (7)$$

with $\delta_a \equiv \Omega_a + 2\Delta_e$. The dynamics of the sensor in the reservoir is purely dephasing under this interaction. However, recent research has demonstrated that dissipative interactions with counter-rotating-wave terms offer greater advantages for quantum sensing compared to dephasing interactions

[39,40]. By applying a two-dimensional magnetic field $H_m = (\hbar B_x \sigma_x + \hbar B_z \sigma_z)/2$ to drive the qubit [41], we can transform Hamiltonian (7) into a dissipative interaction between the sensor and the reservoir. For simplicity, the resonance case, i.e., $\Omega_a + 2\Delta_e - B_z = 0$, will be the main focus, and this requirement can be met by adjusting the magnetic field B_z in the z direction [37]. After making the unitary transform $U_y = e^{-i(\pi/4)\sigma_y}$, the total Hamiltonian becomes

$$\tilde{H} = \frac{\hbar B_x}{2} \sigma_z + \sum_k \hbar \omega_k b_k^\dagger b_k - \sigma_x \sum_k \hbar g_k (b_k + b_k^\dagger). \quad (8)$$

In what follows, the thermometry protocol will be implemented based on Eq. (8), and B_x will be treated as a control parameter.

B. System dynamical evolution

We start by assuming that the entire sensor-reservoir system is initially in a product state given by

$$\rho_{\text{tot}} = |\Psi(0)\rangle\langle\Psi(0)| \otimes \rho_b, \quad (9)$$

where $|\Psi(0)\rangle$ is the initial state of the sensor, and ρ_b is the thermal equilibrium state of the reservoir at temperature T , given by $\rho_b = \prod_k (1 - e^{\beta\omega_k}) e^{-\beta\omega_k b_k^\dagger b_k}$, where $\beta = \hbar/k_B T$ is the inverse temperature. We then use the Zwanzig's projection-operator method to trace out the reservoir in the Liouville's equation of motion, up to second order in the sensor-reservoir coupling [42,43]. This yields the master equation for the sensor's reduced density matrix ρ ,

$$\dot{\rho} = -\frac{i}{\hbar} [H_s, \rho] + \int_0^t d\tau \{ \Phi_T(t-\tau) [\tilde{\sigma}_x(t, \tau) \rho, \sigma_x] + \text{H.c.} \}, \quad (10)$$

with $H_s = B_x \sigma_z/2$. Here, the correlation function for the reservoir is defined as $\Phi_T(t) = \langle \exp(iH_b t/\hbar) \mathcal{B} \exp(-iH_b t/\hbar) \rangle_b$, with $\mathcal{B} \equiv \sum_k g_k (b_k + b_k^\dagger)$ and $\langle \dots \rangle_b = \text{Tr}(\dots \rho_b)$. The unitarily transformed dipole operator in Eq. (10) is $\tilde{\sigma}_x(t, \tau) = \sigma_+ e^{-iB_x(t-\tau)} + \sigma_- e^{iB_x(t-\tau)}$.

Finally, we can write the master equation for the reduced density matrix in terms of the Bloch vector $\hat{S} \equiv (\langle \hat{\sigma}_x \rangle, \langle \hat{\sigma}_y \rangle, \langle \hat{\sigma}_z \rangle)$, without making the rotating-wave approximation (RWA), as follows:

$$\dot{S}_x = -B_x S_y, \quad (11)$$

$$\dot{S}_y = [B_x + 2\Delta(t)] S_x - 2R(t) S_y, \quad (12)$$

$$\dot{S}_z = -2R(t) S_z - 2\Upsilon(t), \quad (13)$$

where

$$R(t) = \int_0^\infty d\omega J(\omega) \coth\left(\frac{\omega}{2T}\right) \frac{\sin[(B_x - \omega)t]}{B_x - \omega}, \quad (14)$$

$$\Upsilon(t) = \int_0^\infty d\omega J(\omega) \frac{\sin[(B_x - \omega)t]}{B_x - \omega}, \quad (15)$$

$$\Delta(t) = \int_0^\infty d\omega J(\omega) \coth\left(\frac{\omega}{2T}\right) \frac{1 - \cos[(B_x - \omega)t]}{B_x - \omega}. \quad (16)$$

$R(t)$ and $\Upsilon(t)$ are the decoherence rates, and $\Delta(t)$ is the resonance shift in energy. In the Markovian limit $t \rightarrow \infty$, we have $R(\infty) = \pi J(B_x) \coth(B_x/2T)$ and $\Upsilon(\infty) = \pi J(B_x)$.

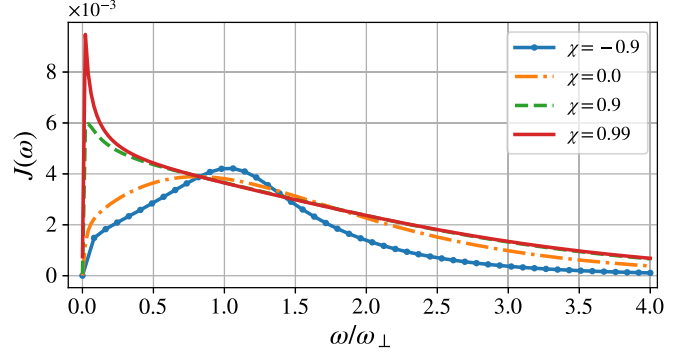


FIG. 2. The spectrum density function $J(\omega)$ given by Eq. (17) for various relative MDDI χ . Here, $\eta = 5$ and $\Theta = 1.5 \times 10^{-2}$.

In terms of the impurity-reservoir coupling parameters g_k , the reservoir spectral density function $J(\omega) \equiv \sum_k |g_k|^2 \delta(\omega - \omega_k)$ can be given as

$$J(\omega) = \Theta \omega_\perp^3 \ell_b^3 \int_0^\infty dk \frac{k^2 e^{-k^2 \ell_a^2/2}}{\omega(k)} \delta[\omega - \omega(k)], \quad (17)$$

where $\omega(k) \equiv \omega_k$ and the dimensionless parameter Θ is defined as $\Theta = n_0 \ell_b^3 a_{ab}^2 (m_a + m_b)^2 / [\pi m_a^2 (\ell_a^2 + \ell_b^2)^2]$. Then, the dynamics of the sensor can be understood by examining the system-environment spectral density $J(\omega)$, which is determined by the parameters of the BEC reservoir and can be adjusted.

As a concrete example, we consider a single ^{23}Na atom immersed in a BEC reservoir composed of ^{164}Dy atoms. The magnetic moment of the reservoir atoms is $\mu_m = 9.9\mu_B$ and the dipolar interaction strength is $a_{dd} \simeq 131a_0$, where μ_B represents the Bohr magneton and a_0 denotes the Bohr radius [44]. The predominantly attractive nature of the dipolar interaction arises from the anisotropy of the MDDI, characterized by the dimensionless parameter χ . However, the effective strength and sign of the dipolar interaction can be modified using techniques such as the fast rotating orienting fields and the Feshbach resonance [45–47]. To facilitate numerical simulations, we introduce dimensionless units. Energy is rescaled in terms of $\hbar\omega_\perp$, time is rescaled in terms of ω_\perp^{-1} , and length is rescaled in terms of $\ell_b = [\hbar/(m_b\omega_\perp)]^{1/2}$. Considering a trap frequency of $\omega_\perp = 300$ Hz and the corresponding oscillator length of $\ell_b = \ell_a \simeq 1.14 \times 10^{-6}$ m, we select a linear density of $n_0 = 10^8 \text{ m}^{-1}$ for the quasi-1D condensate. The s -wave scattering length between Na and Dy atoms is approximately $a_{ab} \sim 5.3$ nm [36,38]. In our numerical simulations presented in this paper, we set $\eta = 5$ and $\Theta = 1.5 \times 10^{-2}$.

To this end, we analyze the spectral density function $J(\omega)$ as a function of the relative strength of MDDI χ , as shown in Fig. 2. At $\chi = 0$, $J(\omega)$ exhibits an approximate Ohmic spectrum with a peak at $\omega = 0.75\omega_\perp$. However, as χ increases, the peak of $J(\omega)$ gradually shifts towards 0, indicating the presence of an attractive interaction. Remarkably, as χ approaches 1, $J(\omega)$ displays a distinct peak near $\omega = 0$. It corresponds to the non-Markovian dissipation rates captured by the frequency $\omega \rightarrow 0$ in Eqs. (11)–(13). These observations sharply contrast with previous studies on 2D dipolar BEC-reservoir systems [36,37], where the dipolar interactions were predominantly repulsive, resulting in the emergence of two

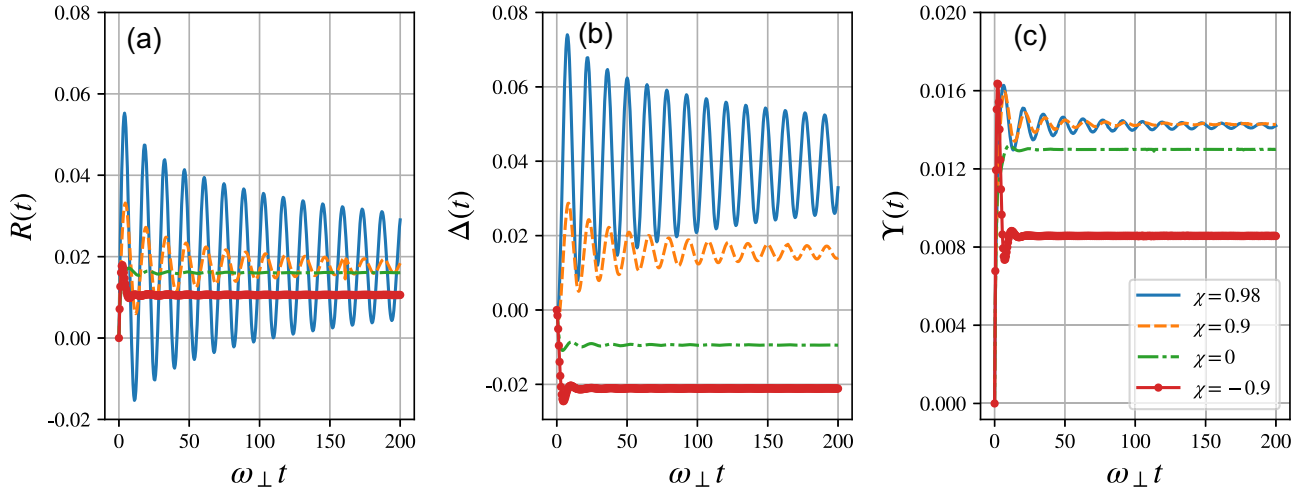


FIG. 3. Dynamic behavior of $R(t)$, $\Delta(t)$, and $\Upsilon(t)$ as a function of time $\omega_{\perp}t$ for different relative MDDI χ . The driving magnetic field strength is chosen as $B_x = 0.45\omega_{\perp}$ and $k_B T / \hbar\omega_{\perp} = 0.2$.

sharp peaks within the intermediate range. Consequently, our current study unveils distinct dynamics compared with the aforementioned Refs. [36,37].

In Fig. 3, we further plot the time-dependent behavior of $R(t)$, $\Delta(t)$, and $\Upsilon(t)$ as a function of $\omega_{\perp}t$ for various χ . The plot illustrates that for $\chi \leq 0$, $R(t)$, $\Delta(t)$, and $\Upsilon(t)$ increase rapidly from zero to a steady state, indicating a Markovian behavior. Conversely, for $\chi > 0.9$, these quantities exhibit damped oscillations that persist for an extended period, signifying a strongly non-Markovian behavior. An important feature of the strongly non-Markovian behavior is the presence of a negative decay rate in $R(t)$, which is evident in the figure. Additionally, the degree of non-Markovianity becomes more pronounced with increasing MDDI strength χ .

C. Non-Markovianity for sensor in a quasi-1D dipolar BEC reservoir

In order to further characterize the non-Markovian nature of the system under consideration, we employ the scheme of measuring the degree of non-Markovianity proposed by Breuer *et al.* [48]. The non-Markovianity, denoted as \mathcal{N} , is defined by

$$\mathcal{N} \equiv \max_{\hat{\rho}_{1,2}(0)} \int_{\sigma > 0} dt \sigma[t; \hat{\rho}_{1,2}(0)]. \quad (18)$$

It quantifies the occurrence of recoherence or information backflow by assessing the rate of change of the trace distance between the physical initial states. Here, $\sigma[t; \hat{\rho}_{1,2}(0)] = \dot{\mathcal{D}}[\rho_1(t), \rho_2(t)]$ represents the rate of change of the trace distance, $\mathcal{D} = \frac{1}{2} \text{Tr}|\rho_1(t) - \rho_2(t)|$, between the states $\rho_1(t)$ and $\rho_2(t)$, considering their respective initial states $\rho_1(0)$ and $\rho_2(0)$. The trace distance between two qubits can be expressed as $\mathcal{D} = \frac{1}{2} |\hat{\mathbf{S}}^{(1)} - \hat{\mathbf{S}}^{(2)}|$. It is important to note that computing Eq. (18) involves determining the maximum value by iterating over the initial states $\hat{\rho}_{1,2}(0)$. Selecting appropriate $\hat{\rho}_{1,2}(0)$ is not a trivial task. However, extensive research has convincingly demonstrated that for a two-level system, the optimal initial states can be chosen as a set of orthogonal pure states, such as $|\pm\rangle = (|e\rangle \pm |g\rangle)/\sqrt{2}$ [48,49]. These states maximize

the non-Markovianity measure as

$$\mathcal{N} = \frac{1}{2} \int dt \{|\sigma[t, \pm]| + \sigma[t, \pm]\}, \quad (19)$$

and the rate of change of the trace distance is $\sigma[t, \pm] = 2\delta S_y^{(\pm)}[\delta S_x^{(\pm)}\Delta(t) - \delta S_y^{(\pm)}R(t)]/\sqrt{(\delta S_x^{(\pm)})^2 - (\delta S_y^{(\pm)})^2}$, with $\delta S_{i=x,y}^{(\pm)} \equiv S_i^{(+)} - S_i^{(-)}$, which depends on the Bloch vectors $\hat{\mathbf{S}}^{(\pm)}$, as well as $\Delta(t)$ and $R(t)$.

By substituting the solution of $\sigma[t, \pm]$ into Eq. (19), we present a plot of the non-Markovianity \mathcal{N} as a function of χ in Fig. 4. As expected, \mathcal{N} increases rapidly when $\chi > 0.9$ and becomes divergent as it approaches $\chi^* = 1$. Consequently, we will focus our subsequent discussion exclusively on cases where $\chi > 1$ in our temperature sensing scheme.

III. NON-MARKOVIAN TEMPERATURE SENSING

The interaction between the sensor and the reservoir, depicted in Fig. 1(b) and described by Eq. (8), effectively encodes the information regarding the temperature of the reservoir into the state of the sensor. Due to the weak coupling between the sensor and the reservoir, the sensor's dynamic behavior can be accurately described by Eqs. (11)–(13). By

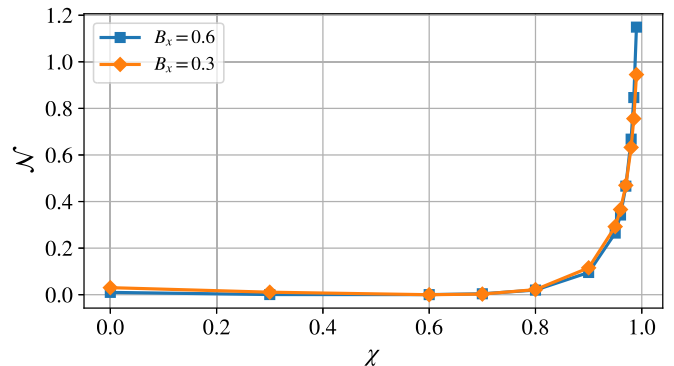


FIG. 4. Non-Markovianity \mathcal{N} as a function of the relative MDDI strength χ . Here, $k_B T / \hbar\omega_{\perp} = 0.2$.

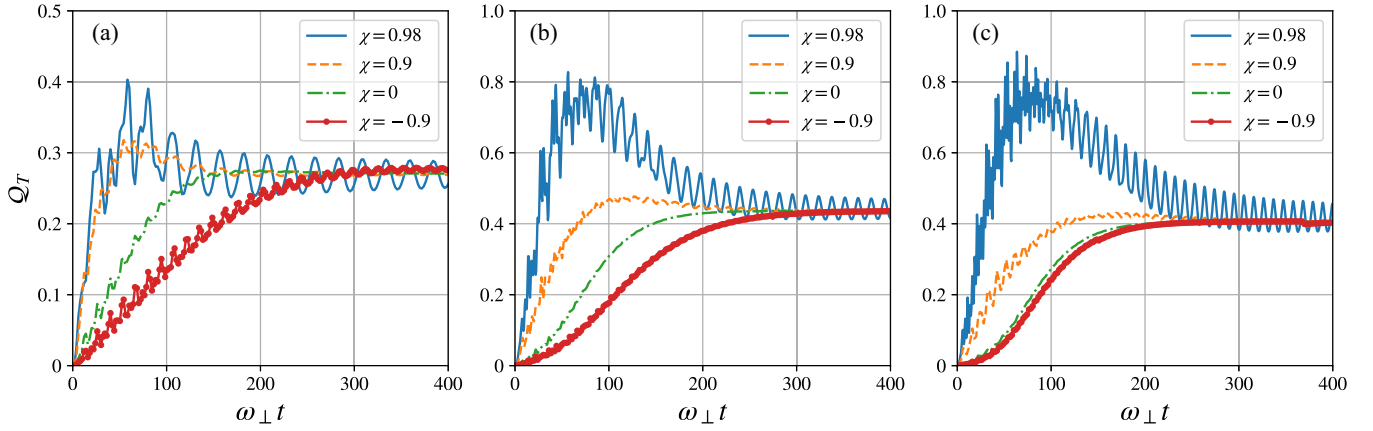


FIG. 5. Dynamic behavior of the QSNR $Q_T(t)$ as a function of time $\omega_{\perp}t$ and different relative MDDI χ for varying external driving magnetic field strength B_x . The driving magnetic field strengths are chosen as (a) $B_x = 0.25\omega_{\perp}$, (b) $B_x = 0.45\omega_{\perp}$, and (c) $B_x = 0.6\omega_{\perp}$. Here the initial state of the sensor is chosen as $|\Psi(0)\rangle = (|e\rangle + |g\rangle)/\sqrt{2}$ and the temperature of the BEC reservoir is $k_B T/\hbar\omega_{\perp} = 0.2$.

measuring specific observables \hat{S} of the sensor, we can acquire valuable insights into the temperature. However, these distinguishing characteristics are not captured by less advanced methodologies.

To assess the precision of our temperature sensing method, we first introduce the quantum parameter estimation theory. As is well known, the ultimate temperature sensing precision is limited by the quantum Cramér-Rao bound, given by $\delta T_{\min} = 1/\sqrt{n\mathcal{F}_T}$, where δT is the mean square error, n is the number of repeated measurements, and \mathcal{F}_T denotes the quantum Fisher information (QFI) with respect to the temperature T . For any two-dimensional density matrix $\rho = \frac{1}{2}(\mathbf{I} + \hat{\mathbf{S}} \cdot \hat{\sigma})$, the QFI \mathcal{F}_T can be easily calculated via [50,51]

$$\mathcal{F}_T = |\partial_T \hat{\mathbf{S}}|^2 + \frac{(\hat{\mathbf{S}} \cdot \partial_T \hat{\mathbf{S}})^2}{1 - |\hat{\mathbf{S}}|^2}. \quad (20)$$

When ρ is a pure state, the above equation further reduces to $\mathcal{F}_T = |\partial_T \hat{\mathbf{S}}|^2$. The temperature sensing performance can be characterized by the optimal relative error,

$$\frac{\delta T_{\min}}{T} = \frac{1}{\sqrt{mQ_T}}, \quad Q_T = T^2 \mathcal{F}_T. \quad (21)$$

Here, Q_T is the QSNR, and a larger QSNR indicates a better temperature sensing performance. It is worth emphasizing that we utilize the QSNR to capture and evaluate the unique characteristics of our temperature sensing method. The accuracy of a temperature measurement relies on various factors, such as the coupling between the sensor and the environment, the strength of the coupling, and the type of environmental noise. Therefore, even with sensing using a single qubit, the conclusions are not obvious. This complexity is particularly prominent when non-Markovian effects are present, making the temperature measurement more intricate.

In what follows, we will investigate a non-Markovian temperature sensing scheme implemented in our proposed model by manipulating B_x and χ .

A. Non-Markovianity enhanced temperature sensing

In terms of Eq. (21), Fig. 5 illustrates the dynamic behavior of the QSNR $Q_T(t)$ as a function of time $\omega_{\perp}t$ and the strength

of the external driving magnetic field B_x for different MDDI values χ . The results provide compelling evidence that attractive interactions ($\chi > 0$) in dipolar BECs lead to an more effective enhancement of Q_T compared to repulsive interactions ($\chi < 0$). Moreover, the observed oscillatory patterns of Q_T , similar to Fig. 4, become more pronounced as χ increases, resulting in higher maximum attainable values of Q_T . Notably, for $\omega_{\perp}t > 100$, the oscillations of Q_T display a regular pattern with an increasing frequency as B_x is increased, as captured by the term $\sin[(B_x - \omega)t]$ in Eqs. (14)–(16). This behavior is particularly significant for $\chi > 0.9$, highlighting the strong non-Markovian effects observed in Fig. 4. These findings suggest that non-Markovian effects have the potential to improve temperature sensing accuracy. However, regardless of the magnitude of χ , the Q_T values converge to a common steady state that is solely dependent on the external driving magnetic field in the long-time regime. Figures 5(a)–5(c) also demonstrate that the Q_T values are highly sensitive to the strength of the external driving magnetic field B_x , indicating that selecting an appropriate driving magnetic field can improve Q_T .

In Fig. 6, we display the maximum achievable QSNR Q_T^{\max} by optimizing the encoding time, as a function of χ , with $B_x = 0.45\omega_{\perp}$ and $0.6\omega_{\perp}$. The results demonstrate a monotonically increasing trend of Q_T^{\max} with values of χ . As χ

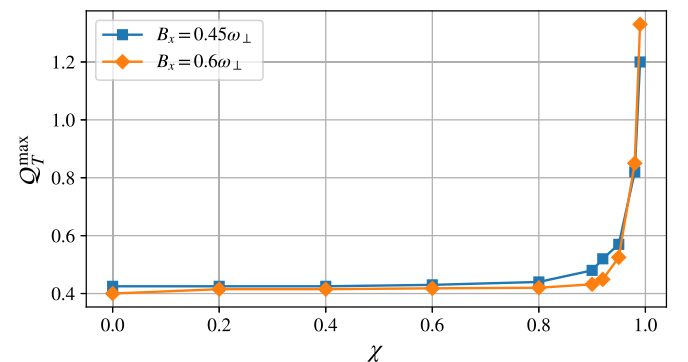


FIG. 6. The maximum QSNR Q_T^{\max} as a function of χ . Here, $k_B T/\hbar\omega_{\perp} = 0.2$.

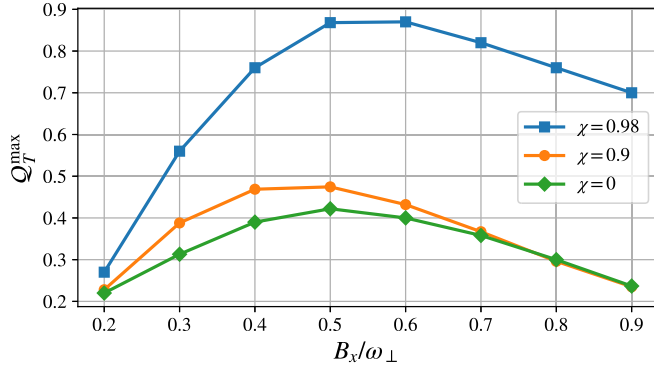


FIG. 7. The maximum QSNR Q_T^{\max} as a function of B_x for different χ . Here, $k_B T / \hbar \omega_{\perp} = 0.2$.

approaches 1, the quantity Q_T^{\max} can reach 1.33, meaning that $(\delta T_{\min}/T)$ can be less than 10% with as few as $n = 100$ measurements. By comparing with Fig. 4, it is clear that this improvement in measurement accuracy follows the same trend as non-Markovianity. This clearly indicates that the enhanced temperature sensing precision is associated with the increase of non-Markovianity.

To better demonstrate the influence of B_x on temperature sensing, Fig. 7 illustrates the impact of B_x on temperature sensing. It presents the maximum achievable QSNR Q_T^{\max} as a function of B_x , considering different values of χ . The graph clearly highlights the presence of an optimal external magnetic field, B_x , for a specific measured temperature T . Moreover, this improvement becomes more pronounced for higher non-Markovianity, i.e., larger values of χ . These findings indicate that adjusting the external magnetic field not only enhances the steady state Q_T , but also significantly improves its dynamic optimal value. For example, under appropriate magnetic fields, such as $B_x = 150$ Hz for $T = 0.458$ nK, the value of Q_T can reach a maximum of 0.85 when $\chi = 0.98$, meaning that the relative error $(\delta T_{\min}/T)$ can be less than 11% in only $n = 100$ measurements.

B. Steady-state results of the temperature sensing

We shall discuss the feature of steady-state QSNR $Q_T(\infty)$ in the long-encoding-time regime. In the long-time limit, based on Eqs. (11)–(13), the Bloch vector can be easily obtained as

$$\begin{aligned} S_x(\infty) &= S_y(\infty) = 0, \\ S_z(\infty) &= -\Upsilon(\infty)/R(\infty) \approx -\tanh(B_x/2T), \end{aligned} \quad (22)$$

which means the long-time steady state of the fully thermalized thermometer can be described by the canonical Gibbs state, $\rho_s(\infty) = \exp(-H_s/T)/\text{Tr}[\exp(-H_s/T)]$.

Then, we have

$$Q_T(\infty) = \left(\frac{B_x}{2T}\right)^2 \left[1 - \tanh^2\left(\frac{B_x}{2T}\right)\right], \quad (23)$$

and the optimal steady-state QSNR $Q_T(\infty) \approx 0.44$ can be obtained when $(\frac{B_x}{2T}) \tanh(\frac{B_x}{2T}) = 1$, which indicates that the optimal relative error can reach 15% with only $n = 100$ measurements.

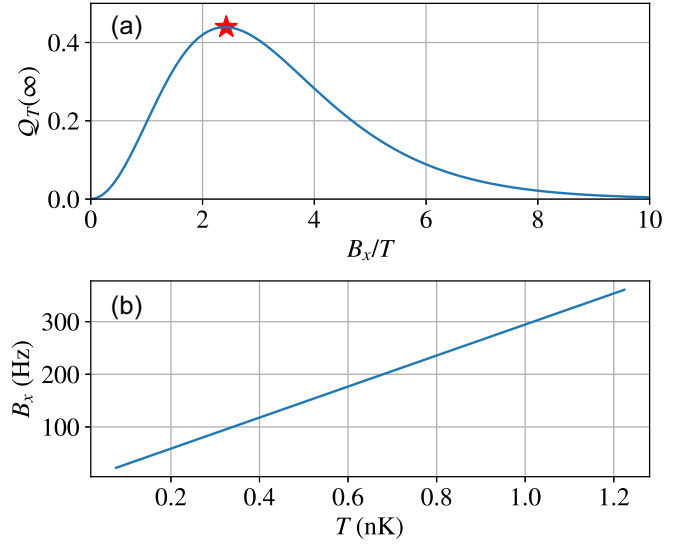


FIG. 8. (a) The steady-state QSNR $Q_T(\infty)$ as a function of B_x/T . The optimal value of QSNR is marked by a red asterisk. (b) The relationship between B_x and T at the optimal point.

It is important to determine the optimal measurement for achieving the highest precision of the estimated parameter in practical experiments. In this study, we have chosen the observable $S_z \equiv \langle \sigma_z \rangle$ as the measurement signal. According to the error propagation formula, the minimum standard deviation for temperature can be expressed as $\delta T = \Delta S_z / |\partial S_z / \partial T|$, where the variance is $\Delta S_z = \sqrt{1 - S_z^2}$. The QSNR Q_T associated with the measurement of population S_z can be obtained from Eq. (22) and yields the relative error for a single measurement ($n = 1$),

$$\frac{\delta T}{T} = \frac{2T}{B_x \sqrt{1 - \tanh^2\left(\frac{B_x}{2T}\right)}} = \frac{1}{\sqrt{Q_T(\infty)}}, \quad (24)$$

which is equivalent to the QSNR presented in Eq. (21).

According to the expression in Eq. (23), Fig. 8(a) shows the variation of the steady-state QSNR $Q_T(\infty)$ with respect to the ratio of the magnetic field along the x direction B_x and the temperature T , in the steady state. As shown in the figure, the steady-state value of $Q_T(\infty)$ is solely determined by the ratio of B_x/T , regardless of the strength of the dipolar interactions. Therefore, by adjusting the magnetic field strength to approximately $B_x/T \approx 2.42$, the temperature sensing sensitivity can be enhanced at any low temperature, as shown in Fig. 8(b).

IV. CONCLUSION

In conclusion, we have presented a method for quantum temperature sensing at extremely low temperatures in a quasi-1D dipolar BEC reservoir, utilizing a magnetic field-driven impurity atom as the quantum sensor. Our proposed model offers highly controllable parameters and the capability to manipulate non-Markovian effects in the environment. These advantageous features make our model an ideal platform for investigating non-Markovian temperature sensing in ultracold atomic gases. Our results highlight the significance

of non-Markovian effects arising from attractive dipolar interactions in the reservoir, which can enhance the efficiency of temperature estimation, indicated by the QSNR. Our proposed scheme can achieve an optimal relative error of less than 10% with just 100 measurements, surpassing the existing methods in the literature [12]. Moreover, we have investigated the steady-state estimation efficiency and observed that it solely relies on the driving magnetic field. Our findings suggest that the optimal relative error can reach 15% with 100 measurements for the case of the steady state at the optimal magnetic field. Furthermore, by adjusting the magnetic field, our approach can achieve high-efficiency temperature sensing for any low temperature. Overall, our proposed method holds great potential for high-resolution quantum thermometry

and can offer a more efficient and accurate approach for temperature sensing at low temperatures.

ACKNOWLEDGMENTS

Q.-S.T. acknowledges support from the National Natural Science Foundation of China (NSFC) (Grant No. 12275077) and the Natural Science Foundation of Hunan Province (Grant No. 2022JJ30277). L.-M.K. is supported by the NSFC (Grants No. 1217050862, No. 12247105, and No. 11935006). J.-B.Y. was supported by NSFC (Grant No. 11905053), Scientific Research Fund of Hunan Provincial Education Department of China (Grant No. 21B0647), and Hunan Provincial Natural Science Foundation of China (Grant No. 2018JJ3006).

-
- [1] I. Bloch, J. Dalibard, and W. Zwerger, *Rev. Mod. Phys.* **80**, 885 (2008).
- [2] A. Leanhardt, T. Pasquini, M. Saba, A. Schirotzek, Y. Shin, D. Kielpinski, D. Pritchard, and W. Ketterle, *Science* **301**, 1513 (2003).
- [3] R. Gati, B. Hemmerling, J. Fölling, M. Albiez, and M. K. Oberthaler, *Phys. Rev. Lett.* **96**, 130404 (2006).
- [4] E. Martín-Martínez, A. Dragan, R. B. Mann, and I. Fuentes, *New J. Phys.* **15**, 053036 (2013).
- [5] C. Sabín, A. White, L. Hackermuller, and I. Fuentes, *Sci. Rep.* **4**, 6436 (2014).
- [6] M. Brunelli, S. Olivares, and M. G. A. Paris, *Phys. Rev. A* **84**, 032105 (2011).
- [7] M. Brunelli, S. Olivares, M. Paternostro, and M. G. A. Paris, *Phys. Rev. A* **86**, 012125 (2012).
- [8] J.-B. Yuan, B. Zhang, Y.-J. Song, S.-Q. Tang, X.-W. Wang, and L.-M. Kuang, *Phys. Rev. A*, **107**, 063317 (2023).
- [9] S. Jevtic, D. Newman, T. Rudolph, and T. M. Stace, *Phys. Rev. A* **91**, 012331 (2015).
- [10] L. Seveso and M. G. A. Paris, *Phys. Rev. A* **97**, 032129 (2018).
- [11] M. T. Mitchison, T. Fogarty, G. Guarnieri, S. Campbell, T. Busch, and J. Goold, *Phys. Rev. Lett.* **125**, 080402 (2020).
- [12] M. Mehboudi, A. Lampo, C. Charalambous, L. A. Correa, M. A. García-March, and M. Lewenstein, *Phys. Rev. Lett.* **122**, 030403 (2019).
- [13] M. M. Khan, M. Mehboudi, H. Terças, M. Lewenstein, and M. A. Garcia-March, *Phys. Rev. Res.* **4**, 023191 (2022).
- [14] M. M. Khan, H. Terças, J. T. Mendonça, J. Wehr, C. Charalambous, M. Lewenstein, and M. A. Garcia-March, *Phys. Rev. A* **103**, 023303 (2021).
- [15] A. Puglisi, A. Sarracino, and A. Vulpiani, *Phys. Rep.* **709-710**, 1 (2017).
- [16] M. Mehboudi, A. Sanpera, and L. A. Correa, *J. Phys. A: Math. Theor.* **52**, 303001 (2019).
- [17] K. V. Hovhannisyán, M. R. Jørgensen, G. T. Landi, Á. M. Alhambra, J. B. Brask, and M. Perarnau-Llobet, *PRX Quantum* **2**, 020322 (2021).
- [18] L. A. Correa, M. Perarnau-Llobet, K. V. Hovhannisyán, S. Hernandez-Santana, M. Mehboudi, and A. Sanpera, *Phys. Rev. A* **96**, 062103 (2017).
- [19] K. V. Hovhannisyán and L. A. Correa, *Phys. Rev. B* **98**, 045101 (2018).
- [20] W.-K. Mok, K. Bharti, L.-C. Kwek, and A. Bayat, *Commun. Phys.* **4**, 62 (2021).
- [21] A. V. Kirkova, W. Li, and P. A. Ivanov, *Phys. Rev. Res.* **3**, 013244 (2021).
- [22] L. A. Correa, M. Mehboudi, G. Adesso, and A. Sanpera, *Phys. Rev. Lett.* **114**, 220405 (2015).
- [23] M. G. A. Paris, *J. Phys. A: Math. Theor.* **49**, 03LT02 (2016).
- [24] P. P. Potts, J. B. Brask, and N. Brunner, *Quantum* **3**, 161 (2019).
- [25] M. R. Jørgensen, P. P. Potts, M. G. A. Paris, and J. B. Brask, *Phys. Rev. Res.* **2**, 033394 (2020).
- [26] K. Berrada, *Phys. Rev. A* **88**, 035806 (2013).
- [27] W. Wu and C. Shi, *Phys. Rev. A* **102**, 032607 (2020).
- [28] W. Wu, S.-Y. Bai, and J.-H. An, *Phys. Rev. A* **103**, L010601 (2021); W. Wu, Z. Peng, S.-Y. Bai, and J.-H. An, *Phys. Rev. Appl.* **15**, 054042 (2021).
- [29] Z.-Z. Zhang and W. Wu, *Phys. Rev. Res.* **3**, 043039 (2021).
- [30] S. Yi and L. You, *Phys. Rev. A* **61**, 041604(R) (2000); **63**, 053607 (2001).
- [31] K. Goral, L. Santos, and M. Lewenstein, *Phys. Rev. Lett.* **88**, 170406 (2002).
- [32] S. Yi, L. You, and H. Pu, *Phys. Rev. Lett.* **93**, 040403 (2004).
- [33] S. Yi, T. Li, and C. P. Sun, *Phys. Rev. Lett.* **98**, 260405 (2007).
- [34] M. Lu, N. Q. Burdick, S. H. Youn, and B. L. Lev, *Phys. Rev. Lett.* **107**, 190401 (2011).
- [35] K. Aikawa, A. Frisch, M. Mark, S. Baier, A. Rietzler, R. Grimm, and F. Ferlaino, *Phys. Rev. Lett.* **108**, 210401 (2012).
- [36] J.-B. Yuan, H.-J. Xing, L.-M. Kuang, and S. Yi, *Phys. Rev. A* **95**, 033610 (2017).
- [37] H. Z. Shen, S. Xu, S. Yi, and X. X. Yi, *Phys. Rev. A* **98**, 062106 (2018).
- [38] Q. S. Tan, J. B. Yuan, G. R. Jin, and L. M. Kuang, *Phys. Rev. A* **96**, 063614 (2017).
- [39] D. Tamascelli, C. Benedetti, H.-P. Breuer, and M. G. A. Paris, *New J. Phys.* **22**, 083027 (2020).
- [40] Z.-Z. Zhang and W. Wu, *Phys. Rev. A* **105**, 043706 (2022).
- [41] H. J. Xing, A. B. Wang, Q. S. Tan, W. X. Zhang, and S. Yi, *Phys. Rev. A* **93**, 043615 (2016).
- [42] H. P. Breuer and F. Petruccione, *The Theory of Open Quantum Systems* (Oxford University Press, Oxford, 2007).
- [43] A. G. Kofman and G. Kurizki, *Phys. Rev. Lett.* **93**, 130406 (2004).

- [44] L. Pitaevskii and S. Stringari, *Bose-Einstein Condensation and Superfluidity* (Oxford University Press, Oxford, 2016).
- [45] S. Giovanazzi, A. Görlitz, and T. Pfau, *Phys. Rev. Lett.* **89**, 130401 (2002).
- [46] T. Lahaye, C. Menotti, L. Santos, M. Lewenstein, and T. Pfau, *Rep. Prog. Phys.* **72**, 126401 (2009).
- [47] A. Griesmaier, J. Stuhler, T. Koch, M. Fattori, T. Pfau, and S. Giovanazzi, *Phys. Rev. Lett.* **97**, 250402 (2006).
- [48] H. P. Breuer, E. M. Laine, and J. Piilo, *Phys. Rev. Lett.* **103**, 210401 (2009).
- [49] I. de Vega and D. Alonso, *Rev. Mod. Phys.* **89**, 015001 (2017).
- [50] W. Zhong, Z. Sun, J. Ma, X. Wang, and F. Nori, *Phys. Rev. A* **87**, 022337 (2013).
- [51] J. Liu, H. D. Yuan, X. M. Lu, and X. G. Wang, *J. Phys. A: Math. Theor.* **53**, 023001 (2020).